MSIM: Multistage Illumination Modeling of Dermatological Photographs for Illumination-Corrected Skin Lesion Analysis

Jeffrey Glaister*, *Student Member, IEEE*, Robert Amelard, *Student Member, IEEE*, Alexander Wong, *Member, IEEE*, and David A. Clausi, *Senior Member, IEEE*

***Abstract*—Melanoma is the most deadly form of skin cancer and it is costly for dermatologists to screen every patient for melanoma. There is a need for a system to assess the risk of melanoma based on dermatological photographs of a skin lesion. However, the presence of illumination variation in the photographs can have a negative impact on lesion segmentation and classification performance. A novel multistage illumination modeling algorithm is proposed to correct the underlying illumination variation in skin lesion photographs. The first stage is to compute an initial estimate of the illumination map of the photograph using a Monte Carlo nonparametric modeling strategy. The second stage is to obtain a final estimate of the illumination map via a parametric modeling strategy, where the initial nonparametric estimate is used as a prior. Finally, the corrected photograph is obtained using the final illumination map estimate. The proposed algorithm shows better visual, segmentation, and classification results when compared to three other illumination correction algorithms, one of which is designed specifically for lesion analysis.**

***Index Terms*—Illumination, melanoma, Monte Carlo sampling, region merging, skin cancer.**

I. Introduction

MELANOMA is a malignant tumor of the melanocytes, a type of cell found in the skin's epidermis [1]. Melanoma most commonly occurs on the trunk or lower extremities and is the most deadly form of skin cancer [1]. In the U.S., 1 in 50 men and women will be diagnosed with melanoma in their lifetime [2]. In 2012, there will be an estimated 76 250 new diagnoses of melanoma and 9180 deaths due to melanoma in the U.S. [3]. More alarming is the increasing incidence rates, particularly among adolescents and young adults. Melanoma is one of the most commonly diagnosed forms of cancer in people of ages 15–30 [4]. Due to the increase in incidence rates, it is costly for dermatologists to manually screen every patient for melanoma. Therefore, there is a need for a system to automatically assess the risk of melanoma from photographs of a patient's skin lesion.

Early work on automated systems to assess the risk of melanoma used dermoscopy images [5]–[8]. These are images that are obtained via a digital dermascope, which is a device that assists dermatologists by magnifying surface detail and filtering surface reflectance. However, only 48% of practicing dermatologists in the U.S. use dermascopes, so the proposed automated systems are difficult to widely adopt [9]. Recent systems use images taken by a standard digital camera, which is more accessible to dermatologists [10], [11]. The photographs are segmented to identify the lesion area, features are extracted from the lesion, and the lesion is classified in terms of risk of melanoma. The problem is that illumination from skin surface reflectance impacts all three of those steps. For example, in Fig. 1, illumination changes across the photographs horizontally or vertically. As a result, healthy skin areas obstructed by shadows appear similar in color as the skin lesion, which results in misclassification of those areas. Illumination correction is an important preprocessing step for skin lesion photographs prior to segmentation and classification algorithms.

Many illumination correction algorithms exist, but they are not designed specifically for skin lesion photographs. Common algorithms correct for illumination based on histogram equalization or the illumination–reflectance model. Histogram equalization adjusts the distribution of pixel intensities and minimizes illumination variation on a global scale [12]. However, this method does not take into account or correct for local illumination variation. The illumination–reflectance model assumes a multiplicative relationship between illumination and reflectance [13]. Algorithms take advantage of this model by estimating the low-frequency illumination component and use it to find the reflectance component. The difference between the algorithms is the initial illumination estimation. One of the earliest algorithms that uses the illumination–reflectance model is the retinex algorithm, which estimates illumination by applying a set of Gaussian filters of different sizes to the image [13], [14]. Other approaches include using morphological operators [15], bilateral filters [16], Monte Carlo sampling [17], or total variation [18] to estimate illumination.

Unfortunately, the existing illumination correction algorithms have difficulties when applied to skin lesion photographs. The

Manuscript received August 15, 2012; revised November 6, 2012; December 5, 2012; accepted December 18, 2012. Date of publication February 1, 2013; date of current version June 24, 2013. This work was supported in part by Agfa Healthcare Inc., Ontario Ministry of Economic Development and Innovation, Ontario Centres of Excellence, and in part by the Natural Sciences and Engineering Research Council of Canada. *Asterisk indicates corresponding author.*

*J. Glaister is with the Vision and Image Processing Lab, Department of Systems Design Engineering, University of Waterloo, ON N2L 3G1, Canada (e-mail: jeffrey.glaister@uwaterloo.ca).

R. Amelard, A. Wong, and D. A. Clausi are with the Vision and Image Processing Lab, Department of Systems Design Engineering, University of Waterloo, ON N2L 3G1, Canada (e-mail: ramelard@uwaterloo.ca; a28wong@engmail.uwaterloo.ca; dclausi@uwaterloo.ca).

Color versions of one or more of the figures in this paper are available online at http://ieeexplore.ieee.org.

Digital Object Identifier 10.1109/TBME.2013.2244596

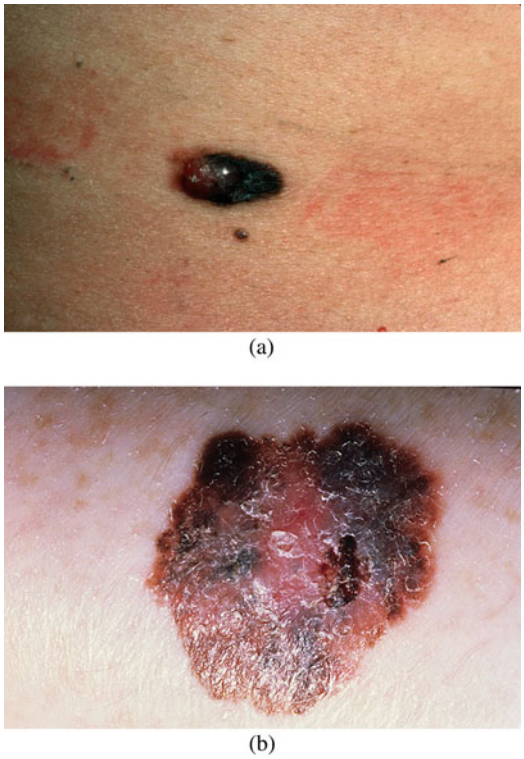

Fig. 1. Examples of illumination variation in skin lesion images. In image (a), the illumination variation changes horizontally, while in image (b), it changes vertically.

skin lesion often appears dark, meaning that illumination correction algorithms can mistake the lesion for image shading [10]. Recent correction algorithms proposed for skin lesion photographs are only applicable for dermoscopy images, where the goal is to normalize color channels or enhance contrast between the lesion and background [19], [20]. One state-of-the-art algorithm specific to illumination correction of skin lesion photographs is proposed by Cavalcanti *et al.*, which fits pixel intensities from the value channel in the hue–saturation–value (HSV) color space to a parametric surface [10], [21]. However, the Cavalcanti *et al.* algorithm only uses a very small subset of pixels from the four corners of the photograph to fit the surface. This can result in over- or underestimation of the required illumination correction.

In this paper, a novel multistage illumination modeling (MSIM) algorithm to correct for illumination variation in skin lesion photographs is proposed. The proposed algorithm, referred to as the MSIM algorithm, follows three stages described in Section II. First, an initial estimate of the illumination map is determined using a nonparametric modeling approach based on Monte Carlo sampling. Second, the final estimated illumination map is found using parametric modeling, using the nonparametric map as a prior. Finally, the illumination variation is removed. The proposed MSIM algorithm extends significantly upon the preliminary results that were presented in [22] through the introduction of an accelerated nonparametric modeling framework in the first stage, and a robust parametric modeling framework in the second stage for improved illumination estimation.

The rest of this paper is organized as follows. In Section III, implementation details about the algorithm are described. In Section IV, the experimental setup is detailed and in Section V, experimental results are given. Finally, in Section VI, there are concluding remarks.

II. Methodology

In this section, the problem of correcting for illumination variations in dermatological photos is formulated. A Monte Carlo nonparametric modeling stage is proposed to solve this problem and a robust parametric modeling stage is proposed to obtain the final estimate of the illumination map.

A. Problem Formulation

Before detailing the MSIM algorithm, it is necessary to derive the underlying illumination model in the skin lesion photographs. In order to derive this model, assumptions are made about the photographs. It is assumed that the photograph is taken in a controlled environment in a doctor's office using a standard camera. The lesion in the photograph is assumed to be illuminated from a single source of white light. Due to these assumptions, only the V (value) channel from the HSV color space [23] is used for illumination correction. The other channels, hue and saturation, are not corrected because the light source is only white light. Furthermore, the skin lesion is found in the center of the photograph.

Finally, the measured V channel pixel intensity is assumed to be the entrywise multiplication of the illumination component and the reflectance component. This is described in (1), where s is defined as a pixel location (x, y), $v(s)$ is the V channel measured intensity, $i(s)$ is the illumination component, and $r(s)$ is the reflectance component. The multiplicative illumination–reflectance model is commonly assumed for illumination correction algorithms [13]. The rest of this section derives the estimate of the illumination component from the measure V channel intensities [24]

$$v(s) = i(s) \cdot r(s). \tag{1}$$

Next, the logarithm transform of both sides in (2) is taken and the multiplicative model becomes an additive model

$$\begin{aligned} \log(v(s)) &= \log(i(s)) + \log(r(s)) \\ v_{\log} &= i_{\log} + r_{\log.} \end{aligned} \tag{2}$$

The estimation of $i_{\log}$ can be seen as an inverse problem. It can be formulated as Bayesian least-squares, where $p(i_{\log}|v_{\log})$ is the posterior:

$$\begin{aligned} \hat{i}_{\log} &= \arg\min_{i_{\log}} \{E((i_{\log} - \hat{i}_{\log})^2)|v_{\log}\} \\ &= \arg\min_{i_{\log}} \Big(\int (i_{\log} - \hat{i}_{\log})^2 \, p(i_{\log}|v_{\log}) di_{\log} \Big). \end{aligned} \tag{3}$$

To minimize the estimate of $i_{\log}$, take the derivative of the arg minargument from (3)

$$\frac{\partial}{\partial \hat{i}_{\log}} \int (i_{\log} - \hat{i}_{\log})^2 \, p(i_{\log}|v_{\log}) di_{\log}$$
$$= \int 2(i_{\log} - \hat{i}_{\log}) \, p(i_{\log}|v_{\log}) di_{\log}. \quad (4)$$

Setting to zero

$$\int i_{\log} \, p(i_{\log}|v_{\log}) di_{\log} = \int \hat{i}_{\log} \, p(i_{\log}|v_{\log}) di_{\log} \quad (5)$$

and simplifying the right-hand side

$$\int \hat{i}_{\log} \, p(i_{\log}|v_{\log}) di_{\log} = \hat{i}_{\log} \int p(i_{\log}|v_{\log}) di_{\log}$$
$$= \hat{i}_{\log} \quad (6)$$

leads to

$$\hat{i}_{\log} = \int i_{\log} \, p(i_{\log}|v_{\log}) di_{\log}$$
$$\hat{i}_{\log} = E(i_{\log}|v_{\log}). \quad (7)$$

As seen in (7), the optimal estimate of the illumination component of an image is the conditional mean of $i_{\log}$ given $v_{\log}$. However, estimating a conditional mean is complex, so a Monte Carlo posterior estimation algorithm is used to estimate $p(i_{\log}|v_{\log})$. Monte Carlo sampling is a nonparametric approach, which means that a parametric model for the posterior distribution $p(i_{\log}|v_{\log})$ does not have to be assumed.

B. Initial Nonparametric Modeling of Illumination

The approach taken for the importance-weighted Monte Carlo sampling [25] for illumination estimation is outlined in this section. As in the previous section, let s be the location of a pixel in the lesion photograph. In this implementation of Monte Carlo sampling, the goal is to determine a set of representative samples Ω and associated importance weights from the pixels s_k in a search space surrounding the pixel of interest s_0. First, a subset of pixels s_k in the search space are selected randomly using a uniform instrumental distribution $Q(s_k|s_0)$. Using a uniform distribution allows all pixels in the search space to have an equal probability of being selected.

For each selected pixel, an acceptance probability $\alpha(s_k|s_0)$ is calculated by comparing the neighborhoods around the selected pixel s_k and pixel of interest s_0, respectively. Let vectors $\boldsymbol{h}_k$ and $\boldsymbol{h}_0$ represent the local neighborhoods around s_k and s_0, respectively. The acceptance probability determines if s_k is a realization of $p(i_{\log}|v_{\log})$. For this implementation, a Gaussian error statistic is used, as shown in (8), where $h_k[j]$ and $h_0[j]$ are the jth sites in the neighborhoods around s_k and s_0, respectively

$$\alpha(s_k|s_0) = \prod_j \frac{\frac{1}{2\pi\sigma} \exp\left[-\frac{(h_k[j]-h_0[j])^2}{2\sigma^2}\right]}{\lambda}. \quad (8)$$

The term λ in the denominator is a normalization term, such that $\alpha(s_k|s_0)$ is 1 if the neighborhoods around s_k and s_0 are identical. The acceptance probability is the product of the probabilities from each site j because elements in the neighborhoods are assumed to be independent. The parameter σ controls the shape of the Gaussian function and is based on local variance. The value of $\alpha(s_k|s_0)$ gives the probability that the pixel s_k is accepted into the set Ω and is used to estimate the posterior distribution $p(i_{\log}|v_{\log})$. Furthermore, $\alpha(s_k|s_0)$ is also the associated importance weight for the accepted pixel. To determine whether to accept pixel s_k, a random value u is drawn from a uniform distribution $U(0,1)$. If $u \leq \alpha(s_k|s_0)$, then s_k is accepted into Ω. Otherwise, s_k is discarded.

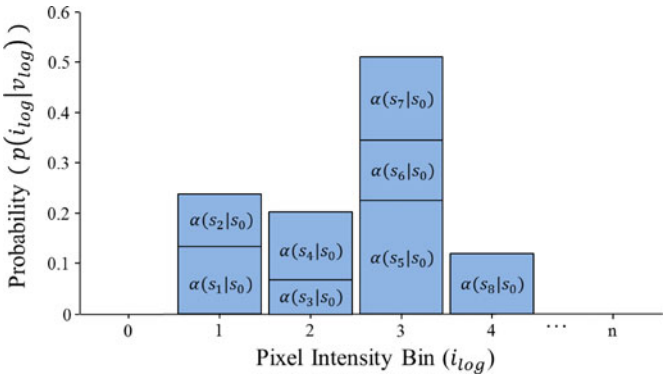

Fig. 2. Sample posterior distribution $\hat{p}\left(i_{\log}|v_{\log}\right)$ built from pixels accepted in the set Ω. Each stacked element corresponds to a pixel s_k in Ω, where the height is $\alpha(s_k|s_0)$ and bin location is s_k. The histogram is normalized so that $\sum_k \hat{p}\left(i_{\log_k}|v_{\log_k}\right) = 1$.

The selection and acceptance process is repeated until the desired number of samples N have been selected from the search space. Then, the posterior distribution is calculated as a weighted histogram. Fig. 2 gives an example of the posterior distribution as a weighted histogram, where each element of the stacked bar chart corresponds to a pixel s_k from the set Ω. The height of the element is equal to the importance weight $\alpha(s_k|s_0)$ and each element is added to the histogram bin corresponding to the value of the pixel intensity s_k. In the example histogram in Fig. 2, the set Ω contains eight pixels (s_1–s_8) and the pixel intensities can range from 0 to n. Finally, the histogram is normalized, so that $\sum_k \hat{p}\left(i_{\log_k}|v_{\log_k}\right) = 1$. Using the estimated posterior distribution, the conditional mean from (7) can be calculated to find the estimate of the illumination component in log-space at pixel s_0. The initial illumination estimate $\hat{i}$ is found by taking the exponential of $\hat{i}_{\log}$. For testing, a 21×21 search space and 7×7 neighborhood were used.

C. Final Parametric Modeling of Illumination

After the initial nonparametric model stage, the lesion appears as shading in the initial illumination estimate $\hat{i}$ because the lesion is darker than its surroundings, thus leading to a poor estimate within the lesion area. Therefore, using the initial illumination map to correct for illumination variation results in the lesion being greatly brightened to reduce the contrast between the lesion and surrounding skin. To address this issue, parametric modeling of illumination via a quadratic surface model is performed using the initial nonparametric illumination

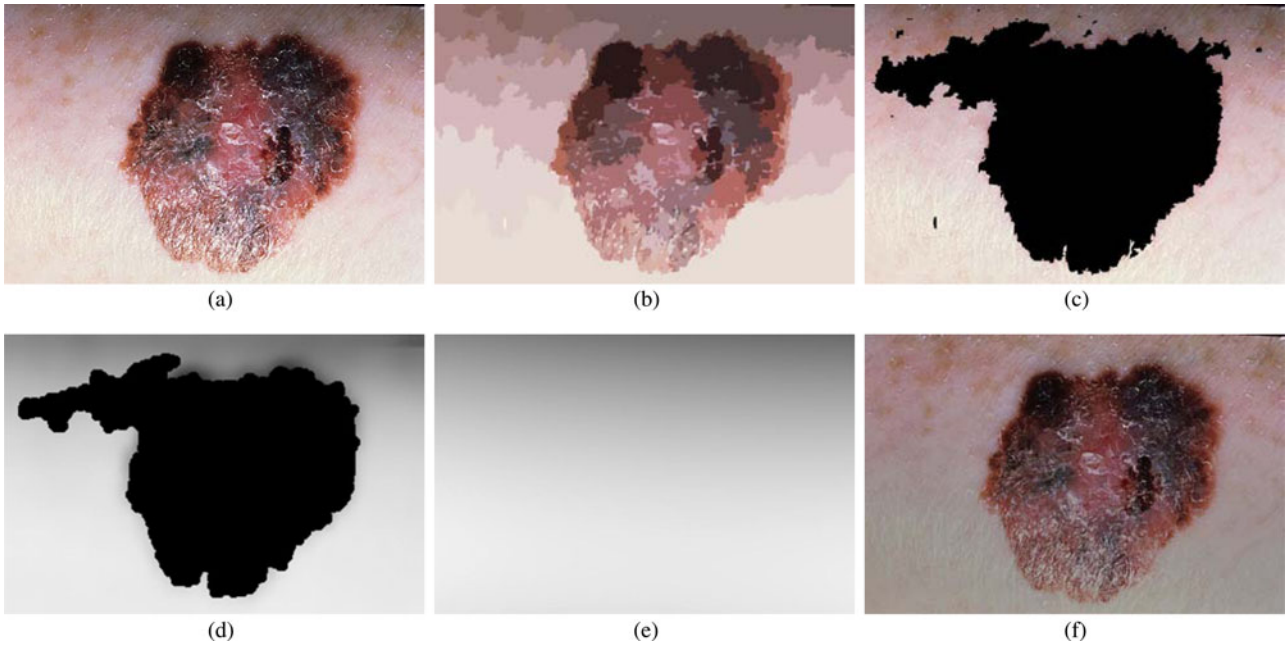

Fig. 3. Methodology to calculate illumination map: (a) original photograph of a skin lesion with illumination variation; (b) segmentation map; (c) regions included in the subset of skin pixels, where pixels black in color are not classified as normal skin; (d) initial illumination map estimated via nonparametric modeling using Monte Carlo sampling; (e) final illumination map determined by using (d) as a prior to the parametric surface model; (f) photograph corrected for illumination variation using the MSIM algorithm.

estimate as a prior to obtain the final illumination map. This final stage uses assumptions made about the lighting conditions to learn a surface model based on the initial illumination estimates corresponding to the healthy skin pixels and find the correct illumination map for the lesion area.

The first step in the final stage is to obtain a rough estimate of the healthy skin pixels and lesion pixels. A segmentation algorithm is applied to the original photograph and any regions that touch the border are classified as healthy skin. As previously assumed, the lesion is typically centered in the photograph. Therefore, using this heuristic to classify regions gives a rough estimate of which pixels are skin. Fig. 3(b) shows an example of the segmentation results and Fig. 3(c) shows the areas classified as skin using the heuristic. It is not necessary to have a perfect segmentation algorithm because these pixels are only used to fit the surface model. The segmentation algorithm used in the implementation is statistical region merging (SRM) and is described in Section III-B.

The second step is to learn a quadratic surface model (9) based on the initial nonparametric illumination estimate corresponding to the healthy skin pixels [21]

$$i'(x,y) = P_1x^2 + P_2xy + P_3y^2 + P_4x + P_5y + P_6. \quad (9)$$

Using this model, the parameters of the final illumination map are estimated using maximum likelihood estimation based on the initial estimate $\hat{i}$ and the set of skin pixels S. However, to minimize the effect of outliers on the illumination map, a robust fitting algorithm using the Tukey biweight is implemented, as shown in (10), where c is the tuning constant [26]

$$\hat{i}' = \arg\min_{\hat{i}'} \sum_{s\in S} \rho(\hat{i}(s) - \hat{i}'(s)) \quad (10)$$

$$\text{where } \rho(z) = \begin{cases} \frac{c^2}{6}(1-[1-(z/c)^2]^3), & \text{for } |z| \le c \\ \frac{c^2}{6}, & \text{for } |z| > c. \end{cases}$$

The value for c was set to 4.6851, which is the standard Tukey biweight tuning constant. Fig. 3(d) shows the pixel intensities from the initial illumination map that are used to fit the surface and Fig. 3(e) shows the resulting surface after being fit.

D. Reflectance Map Estimation

The illumination–reflectance model assumes that the V channel is the entrywise multiplication of the illumination and reflectance components. Therefore, the reflectance map can be estimated by dividing the original V channel pixel intensity $v(s)$ by the final estimated illumination map $\hat{i}'(s)$. The reflectance channel is combined with the original hue and saturation channels to correct the photograph for illumination variation. Fig. 3(f) shows an example of a corrected photograph.

III. Implementation

In this section, the implementation details of the MSIM algorithm are described, including segmentation and additional steps added for optimization.

A. Optimization

The Monte Carlo algorithm can be computationally complex, so two steps are added prior to the first stage of illumination estimation to increase computation speed. First, the photograph is downscaled by a factor of 2, and then the Monte Carlo illumination estimation is applied to the smaller image. Since

illumination is of low frequency, the loss of details does not impact the final illumination estimation. The initial nonparametric illumination estimation is rescaled to the original photograph's size before obtaining the parametric illumination estimation.

The second optimization step is to estimate the pixels that belong to healthy skin and only apply the Monte Carlo sampling algorithm to those pixels. In the final parametric illumination map, only the initial illumination estimate associated with healthy skin pixels is considered in the robust fitting algorithm. Therefore, there is no need to calculate the initial estimate for lesion pixels. The method to find the healthy skin pixels is described in the next section. A morphological closing operator with a small disk structuring element is applied to the skin pixel map to fill in gaps.

B. SRM

A segmentation algorithm is applied to the original color photograph to classify pixels as healthy skin or lesion. The segmentation algorithm implemented is the SRM [27], which tends to oversegment an image. SRM groups pixels of similar color into segments and any segments touching the border are classified as healthy skin and are added to the set S. Since the lesion is assumed to be found in the center of the photograph, only segments corresponding to healthy skin are found near the borders of the photograph.

SRM uses two important steps to perform segmentation of a color image. First, the image is set up as a four-connected graph. This motivates the sorting step, where pairs of pixels are organized based on the maximum difference in the RGB values. Pixels that are closer in color are merged first. As pixels are merged, they are treated as regions. Second, a merging predicate is introduced, which will merge two regions based on similarity between the average RGB intensities of the two regions of interest. The SRM algorithm contains a single tunable parameter Q which was set to 256.

C. Summary of the MSIM Algorithm

1) Apply SRM to the original RGB photograph (see Section III-B) to classify healthy skin pixels.
2) Downscale V channel of the original HSV image by factor 2 (see Section III-A).
3) Iterating through each pixel of interest s_0 that is part of the healthy skin pixel set S in the downscaled image, randomly draw a sample s_k from a search space around s_0 using a uniform instrumental distribution.
4) Compute acceptance probability $\alpha(s_k|s_0)$ using (8).
5) Generate a random value u from a uniform distribution $U(0,1)$. If $u \leq \alpha(m_k|m_0)$, include k in the set of accepted samples Ω with an importance weight equal to $\alpha(s_k|s_0)$. Otherwise, s_k is discarded.
6) Repeat steps 3–5 until the desired number of samples N are selected from the search space.
7) Estimate the posterior distribution $\hat{p}\,(i_{\log}|v_{\log})$ based on the samples in Ω and their importance weights.
8) Compute the initial illumination map estimate in log-space $\hat{i}_{\log}$ for pixel s_0 as the conditional mean in (6). Rescale the initial illumination map to the dimensions of the original image.
9) Using the initial illumination map corresponding to healthy skin pixels, calculate the parametric surface using a robust fitting algorithm to obtain the final estimated illumination map.
10) Estimate the reflectance map (see Section II-D) and replace the original V channel with the reflectance map to obtain the corrected image.

IV. Experimental Setup

This section describes the experimental setup to compare the MSIM algorithm to other illumination correction algorithms. The three state-of-the-art algorithms used for comparison are the retinex algorithm (as implemented in [28]), morphological illumination estimation [15], and Cavalcanti *et al.*'s algorithm [10]. Of the three comparison algorithms, only Cavalcanti *et al.*'s algorithm is designed specifically for skin lesion images. To compare algorithms, the illumination-corrected photographs were normalized by adjusting the average V channel values of the healthy skin class to be equal. A manual ground truth segmentation was used to obtain the true classification of the pixels. Normalization allows a fair comparison as the images are adjusted to have a similar dynamic range of skin pixel intensities.

A set of 64 photographs tested were from the Dermatology Information System database [29] and 127 were from the DermQuest database [30]. One hundred and eight images tested had melanomas, while 83 images had other types of skin lesions. Some examples of the types of photographs tested are shown in Fig. 4.

The resulting images were first compared visually. The quantitative experiments compare the effects of illumination correction on segmentation and classification. Receiver operating characteristic (ROC) curves were calculated and compared for each image, using a simple threshold algorithm to segment the photograph into lesion and nonlesion. Finally, a lesion classification framework was built and the images were used to train and classify other images of skin lesions.

V. Experimental Results

A. Visual Comparison Results

Examples of corrected images, corresponding to the uncorrected images in Fig. 4, are shown in Fig. 5 . First, Cavalcanti *et al.* and MSIM algorithms maintain a consistent lesion color after illumination correction, while the retinex and morphological algorithms cause a change in lesion color. This is seen most prominently in Fig. 5(a), (b), (e), and (g). This occurs because without the parametric modeling step, the lesion is mistaken as a shadow and the illumination correction algorithm brightens that area. As a result, the contrast between skin and lesion is decreased, which can affect segmentation. Furthermore, in cases where there is more complex skin texture and illumination, such as Fig. 5(d) and (i), the illumination variation is not removed by Cavalcanti *et al.*'s algorithm, but is removed by the MSIM algorithm. This is due to MSIM's parametric modeling stage using a greater number of pixels to fit the surface compared

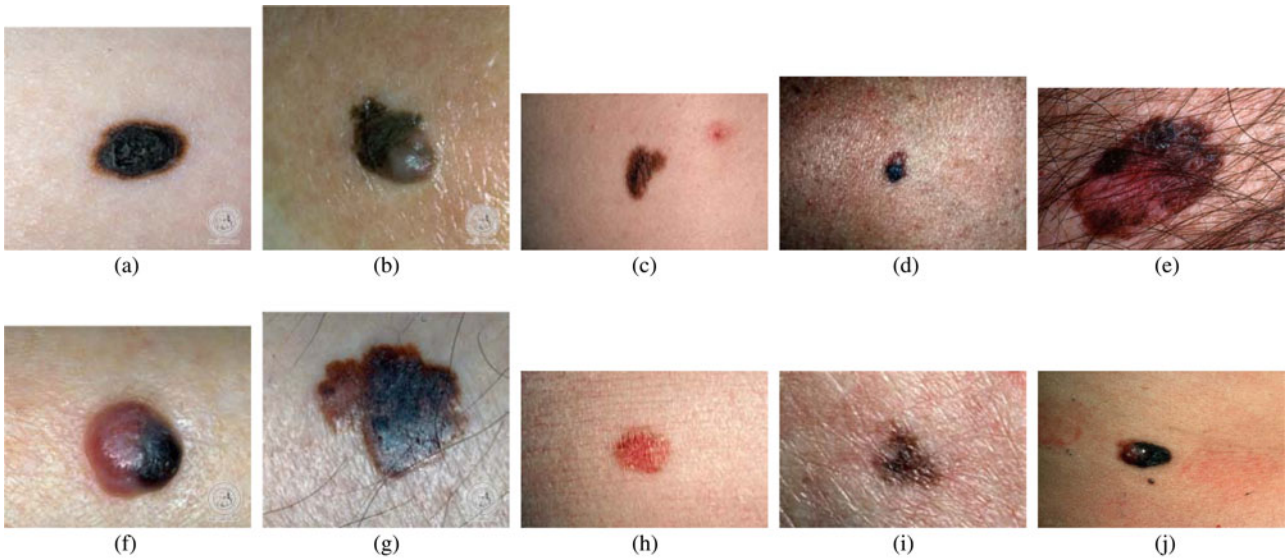

Fig. 4. Examples of uncorrected images with illumination variation. Images (d)–(g), (i), and (j) are cases where the patient has melanoma and images (a)–(c) and (h) are cases where the patient does not. Images (a), (b), (f), and (g) are from the DermIS database and images (c)–(e) and (h)–(j) are from the DermQuest database.

to the Cavalcanti *et al.* Using more pixels allows for a better surface fit and visibly better correction results.

Fig. 6 shows an example photograph with complicated, highly oversaturated illumination variation that is not corrected satisfactorily by all of the tested methods. This is not surprising as the light source reflected off the center of the lesion completely saturates the photograph in that area, making it challenging for all tested methods to model the illumination in that region. Note that the proposed MSIM algorithm is able to correct some of the illumination variation excluding the aforementioned oversaturated region.

B. Segmentation Results

The uncorrected and corrected images were compared based on the ability to segment lesion and normal skin pixels. The segmentation algorithm used is described in [21]. Separate thresholds are found for the R, G, and B color channels and if a pixel's intensity is below those thresholds in two channels, then that pixel is classified as lesion. Furthermore, finding the optimal thresholds for each photograph greatly depends on the dynamic range and contrast of the images. Unlike the algorithm in [21] which finds Otsu's threshold for each channel, a subset of all possible values for the thresholds is tested and ROC curves are determined.

ROC curves plot the true-positive rate (TPR) versus false-positive rate (FPR) found for different thresholds [31]. The TPR is the proportion of true positives of all positives and the FPR is the proportion of false positives of all negatives. An ideal ROC curve passes through the point where $\mathrm{TPR} = 1$ and $\mathrm{FPR} = 0$, meaning that there is perfect segmentation for some threshold value. Otherwise, curves that are closer to the top left of the graph correspond to a more accurate segmentation. The ROC curves are shown in Fig. 7.

To quantify the ROC curve, the area under the curve (AUC) is calculated. A higher AUC also corresponds to more accurate segmentation results. The AUCs for the full dataset and "melanoma" and "nonmelanoma" subsets are shown in Table I.

From Fig. 7 and Table I, the MSIM algorithm performs the best for image segmentation, followed by Cavalcanti *et al.*'s algorithm. This is because the MSIM algorithm uses a larger set of normal skin pixels to fit the parametric surface compared to Cavalcanti *et al.*'s algorithm. The other two algorithms do not fit any surface for illumination correction. Therefore, the images are harder to separate using segmentation algorithms.

C. Classification Results

Using images corrected by each illumination correction algorithm, a separate classifier was trained to segment the image, extract features based on the ABCD scale of dermatoscopy [32], and assess the lesion for the risk of melanoma. The segmentation algorithm and features used are implemented from [10]. Of the set of 52 features, 11 characterize asymmetry, 12 characterize border irregularity, 25 characterize color, and 4 characterize differential structure. A support vector machine (SVM) classifier was used for training and testing. The SVM algorithm was implemented using A Library for Support Vector Machines (LIBSVM) [33], with a linear kernel and the soft-margin cost parameter set to 1. The feature scores were normalized to have zero mean and unit variance. To compare results from the different correction methods, the sensitivity, specificity, and accuracy are used as metrics using a leave-one-out cross-validation scheme. Only the 127 images from the DermQuest database were used for classification, because they had appropriate image quality and resolution.

The classification results using the uncorrected and corrected lesion images are shown in Table II. The MSIM and Cavalcanti *et al.*'s algorithms have the highest sensitivity, while MSIM has the highest specificity and accuracy. This is partly due to the illumination correction algorithm increasing the separability of

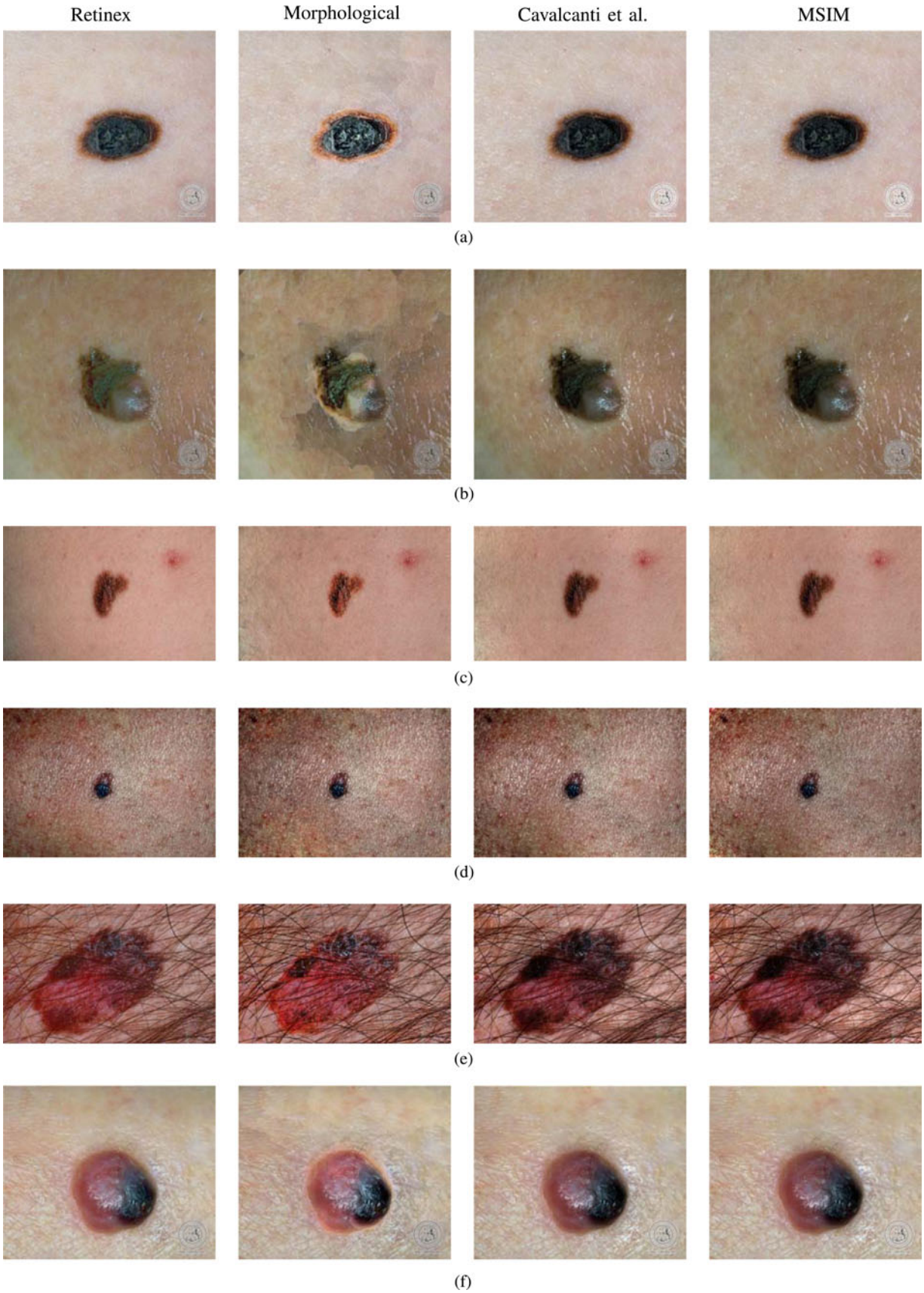

Fig. 5. Corrected skin lesion images, corresponding to the images in Fig. 4. In images (a), (b), (e), and (g), the retinex and morphological algorithms cause a change in the lesion color and a decrease in contrast between lesion and skin. In images (d) and (i), Cavalcanti *et al.*'s algorithm does not adequately correct for illumination variation, while the MSIM algorithm does.

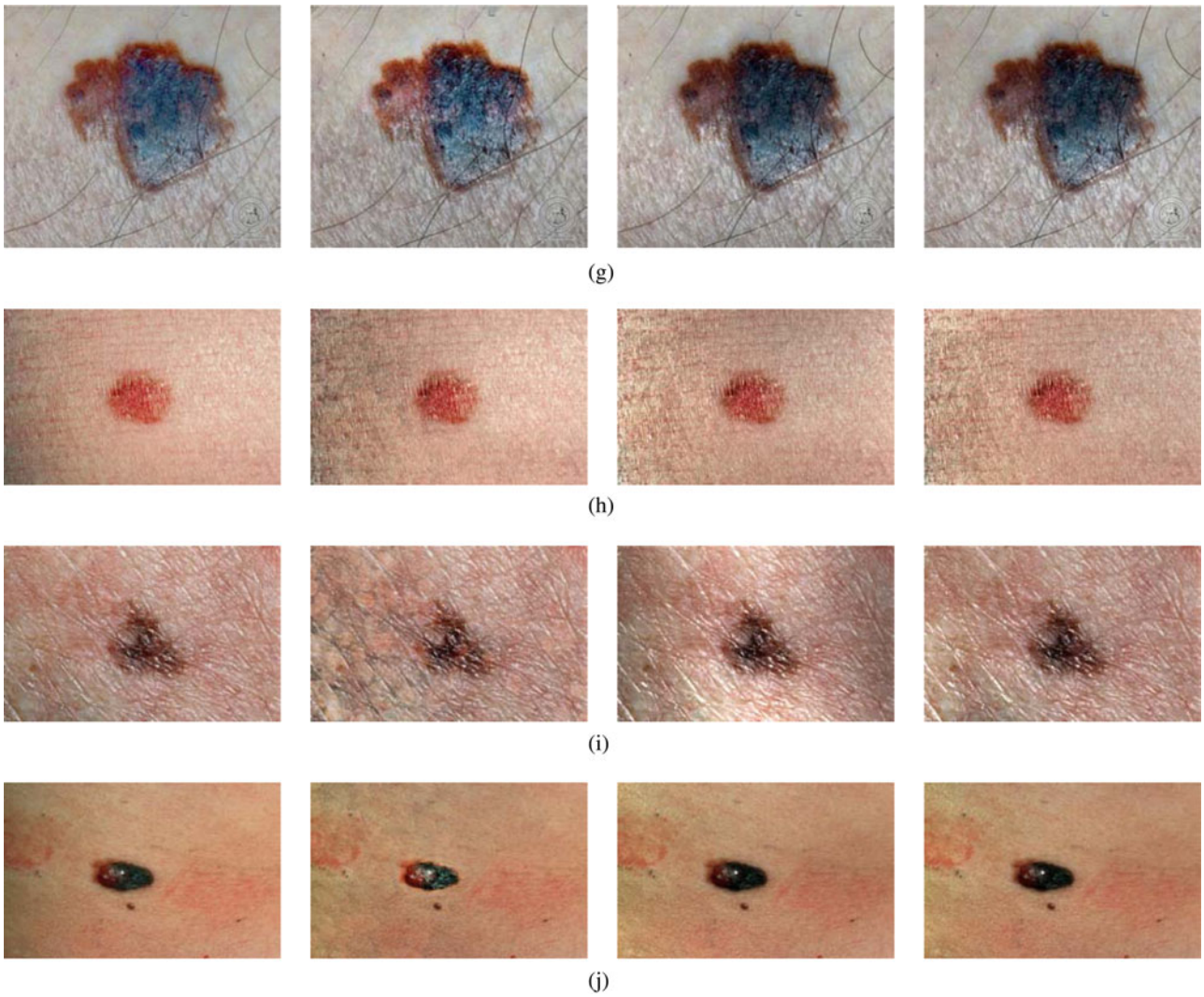

Fig. 5. (Continued). Corrected skin lesion images, corresponding to the images in Fig. 4, cont.

Fig. 6. Example of the limitations of the tested illumination correction algorithms. None of the tested illumination correction algorithms are able to model and correct the light reflected off of the center of skin lesion which oversaturates the photograph in that area. Note that the proposed MSIM algorithm is able to correct some of the illumination variation excluding the aforementioned oversaturated region.

the lesion and normal skin, allowing for more accurate segmentation. Eleven of the features used depend on the morphology of the segmentation border. Second, the illumination correction algorithm can increase class separability using intensity-based features.

D. Comparison of MSIM Versus Parametric Illumination Modeling

Given that the proposed MSIM algorithm involves a nonparametric modeling stage and a parametric modeling stage, an investigation into the importance of performing both stages was conducted by comparing the results obtained: 1) using solely the parametric modeling stage and 2) using both the nonparametric and parametric modeling stages. One of the key benefits with using an initial nonparametric modeling stage is that this type of modeling strategy is more robust to the presence of outlier detail in the photograph than a purely parametric modeling strategy. This robustness to outlier detail is particularly important in photographs with significant amounts of hair, which can lead to very poor illumination estimates if a purely parametric

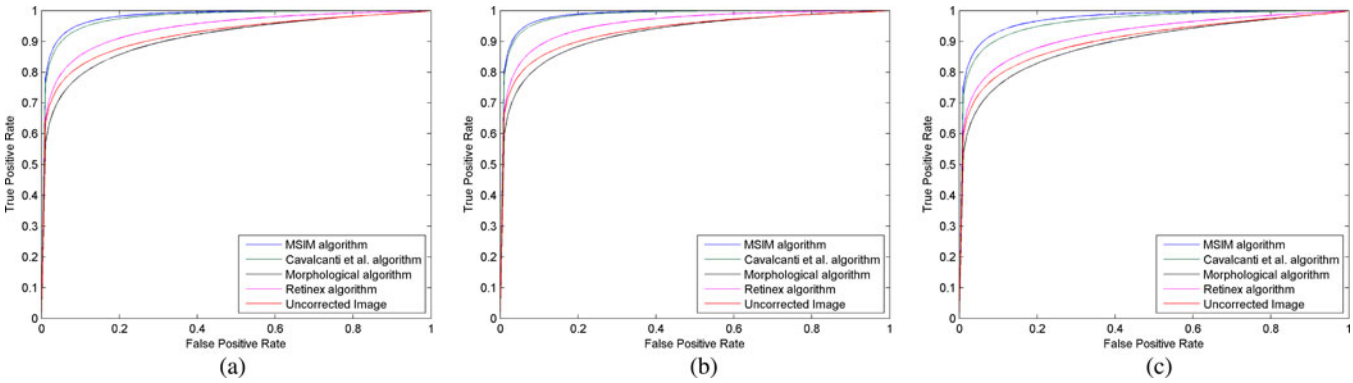

Fig. 7. ROC curves corresponding to segmentation results using different thresholds for melanoma and nonmelanoma skin lesion images. Graph (a) uses the result from the entire dataset, while graphs (b) and (c) use only the melanoma or nonmelanoma images, respectively. (a) All. (b) Melanoma. (c) Nonmelanoma.

TABLE I
AREA UNDER ROC CURVES FOR UNCORRECTED AND CORRECTED SKIN LESION IMAGES

Type	Uncorrected	Retinex	Morphological	Cavalcanti et al.	MSIM
All AUC	0.9225	0.9435	0.9114	0.9788	**0.9830**
Melanoma AUC	0.9368	0.9581	0.9278	0.9850	**0.9871**
Non-melanoma AUC	0.9058	0.9239	0.8934	0.9655	**0.9750**

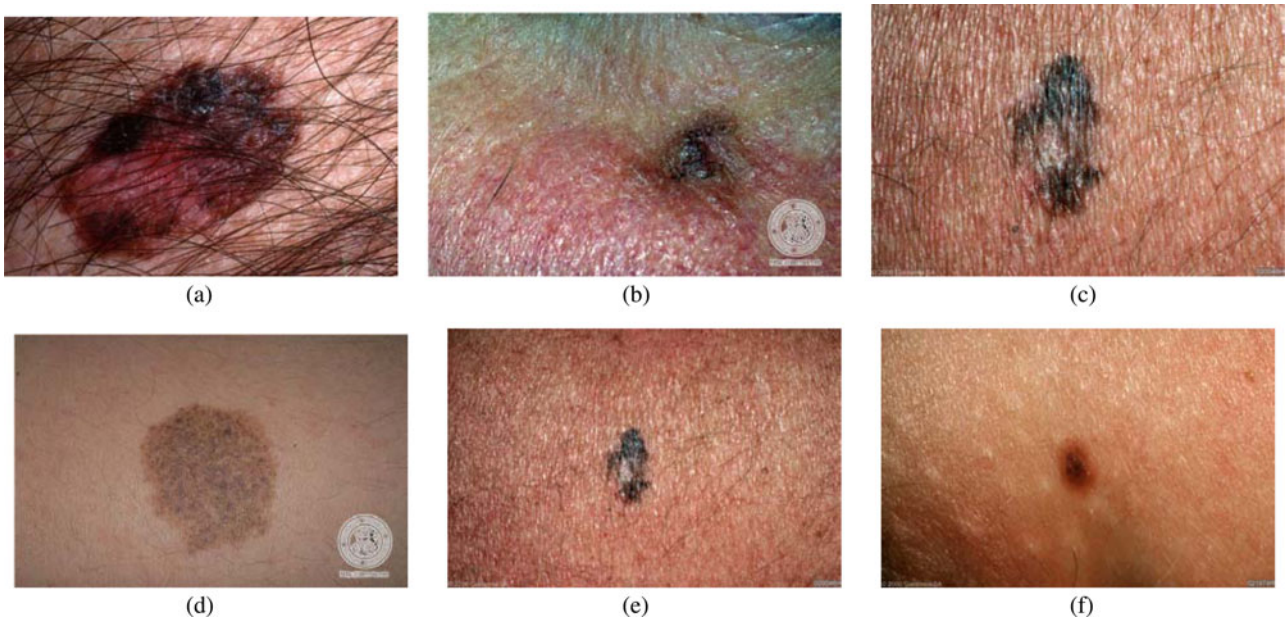

Fig. 8. Subset of photographs with significant artifacts. These images were used to compare the results of using both stages of the MSIM algorithm to correct for illumination variation compared to using solely the parametric modeling stage.

modeling approach is employed. The use of an initial outlier-robust nonparametric estimate as a prior to a parametric modeling stage allows for significantly improved illumination estimates.

A subset of six photographs with significant artifacts were corrected using both stages of the MSIM algorithm and using solely the parametric modeling stage. The subset included photographs from both the Dermatology Information System and DermQuest databases and photographs with melanoma and with nonmelanoma lesions. The photographs in this subset are shown in Fig. 8. To quantify the effect of illumination correction on the images, the coefficient of variation of the skin pixels was calculated for the resulting images using both algorithms. Coefficient of variation has been used to quantify the performance of other illumination correction algorithms [34]. It compares the mean skin pixel intensity to the variance of the skin pixel intensities and is given in (11) [34]. A lower coefficient of variation after correction is desirable, as the only variation in pixel intensities

TABLE II
CLASSIFICATION RESULTS USING UNCORRECTED AND CORRECTED LESION IMAGES

Correction Algorithm	Sensitivity	Specificity	Accuracy
Uncorrected	69.2%	63.3%	65.9%
Retinex	69.7%	75.0%	72.2%
Morphological	71.2%	61.7%	66.7%
Cavalcanti et al.	**74.2%**	77.9%	76.0%
MSIM	**74.2%**	**83.3%**	**78.6%**

should be from texture characteristics. The pixel intensities of healthy skin in the images were normalized so that the dominant cause of a change in coefficient of variation is due to a change in variance

$$C = \frac{\sigma}{\mu}. \tag{11}$$

The average coefficient of variation of the set of photographs corrected using both stages was 0.1442 and the average coefficient of variation of the images corrected using only the parametric modeling stage was 0.1501. Therefore, using both stages resulted in a lower coefficient of variation than if only the parametric modeling stage is performed.

ROC curve analysis was performed on the subset, as described in Section V-B. The area under the ROC curve (AUC) for the images corrected using both stages was 0.9085, while the AUC for the images corrected using only the parametric modeling stage was 0.8966. Since the ROC AUC is higher for the subset of images corrected using both stages, it indicates that the skin pixels and lesion pixels are more separable in those corrected images. From the coefficient of variation and ROC results, the combination of a nonparametric modeling stage with a parametric modeling stage results in a final image that is noticeably better corrected for illumination variation.

VI. CONCLUSION

A novel MSIM algorithm has been proposed to correct illumination variation in dermatological skin lesion photographs. The proposed MSIM algorithm first determines a nonparametric model of illumination using Monte Carlo sampling. Next, a parametric model assuming a quadratic surface model is used to determine the final illumination estimate based on a subset of pixels from the nonparametric illumination estimate. Finally, by using the final illuminate estimate, the reflectance component of the photograph is calculated and a new photograph is constructed which is corrected for illumination. Experimental testing compared the uncorrected images with corrected images using the proposed and three state-of-the-art illumination correction algorithms. The images were compared visually and by applying segmentation and classification algorithms. The MSIM algorithm produced images that were more separable for lesion segmentation, based on the area under the ROC curve. The images corrected by the MSIM algorithm also performed better for training a classifier to assess the risk of melanoma. The classifier trained using MSIM-corrected images had the highest sensitivity, specificity, and accuracy.

REFERENCES

[1] Public Health Agency of Canada. (2012, Jul.). *Melanoma Skin Cancer* [Online]. Available: http://www.phac-aspc.gc.ca/cd-mc/cancer/melanoma_skin_cancer-cancer_peau_melanome-eng.php

[2] N. Howlader, A. M. Noone, M. Krapcho, N. Neyman, R. Aminou, S. F. Altekruse, C. L. Kosary, J. Ruhl, Z. Tatalovich, H. Cho, A. Mariotto, M. P. Eisner, D. R. Lewis, H. S. Chen, E. J. Feuer, and K. A. Cronin, (2012, Jul.). SEER cancer statistics review, 1975–2009 (vintage 2009 populations). *Nat. Cancer Inst.* [Online]. Available: http://seer.cancer.gov/statfacts/html/melan.html

[3] R. Siegel, D. Naishaand, and A. Jemal, "Cancer statistics, 2012," *Cancer J. Clin.*, vol. 62, no. 1, pp. 10–29, 2012.

[4] C. Herzog, A. Pappo, M. Bondy, A. Bleyer, and J. Kirkwood, "Malignant melanoma," in *Cancer Epidemiology in Older Adolescents and Young Adults 15 to 29 Years of Age, Including SEER Incidence and Survival: 1975-2000*, A. Bleyer, M. OLeary, R. Barr, and L. A. G. Ries, Eds. Bethesda, MD, USA: Nat. Cancer Inst., 2006, pp. 53–64.

[5] M. E. Celebi, H. A. Kingravi, B. Uddin, H. Iyatomi, Y. A. Aslandogan, W. V. Stoecker, and R. H. Moss, "A methodological approach to the classification of dermoscopy images," *Comput. Med. Imag. Graph.*, vol. 31, no. 6, pp. 362–373, 2007.

[6] S. W. Menzies, L. Bischof, H. Talbot, A. Gutenev, M. Avramidis, L. Wong, S. K. Lo, G. Mackellar, V. Skladnev, W. McCarthy, J. Kelly, B. Cranney, P. Lye, H. Rabinovitz, M. Oliviero, A. Blum, A. Varol, B. De'Ambrosis, R. McCleod, H. Koga, C. Grin, R. Braun, and R. Johr, "The performance of solarscan: An automated dermoscopy image analysis instrument for the diagnosis of primary melanoma," *Arch. Dermatol.*, vol. 141, no. 11, pp. 1388–1396, Nov. 2005.

[7] H. Iyatomi, H. Oka, M. E. Celebi, M. Hashimoto, M. Hagiwara, M. Tanaka, and K. Ogawa, "An improved internet-based melanoma screening system with dermatologist-like tumor area extraction algorithm," *Comput. Med. Imag. Graph.*, vol. 32, pp. 566–579, 2008.

[8] H. Ganster, A. Pinz, R. Rührer, E. Wildling, M. Binder, and H. Kittler, "Automated melanoma recognition," *IEEE Trans. Med. Imag.*, vol. 20, no. 3, pp. 233–239, Mar. 2001.

[9] H. C. Engasser and E. M. Warshaw, "Dermatoscopy use by US dermatologists: A cross-sectional survey," *J. Amer. Academy Dermatol.*, vol. 63, no. 3, pp. 412–419, Sep. 2010.

[10] P. G. Cavalcanti and J. Scharcanski, "Automated prescreening of pigmented skin lesions using standard cameras," *Comput. Med. Imag. Graph.*, vol. 35, pp. 481–491, 2011.

[11] J. F. Alcon, C. Ciuhu, W. ten Kate, A. Heinrich, N. Uzunbajakava, G. Krekels, D. Siem, and G. De Haan, "Automatic imaging system with decision support for inspection of pigmented skin lesions and melanoma diagnosis," *IEEE J. Sel. Topics Signal Process.*, vol. 3, no. 1, pp. 14–25, Feb. 2009.

[12] S. Shan, W. Gao, B. Cao, and D. Zhao, "Illumination normalization for robust face recognition against varying lighting conditions," in *Proc. IEEE Int. Workshop Anal. Model. Faces Gesture*, Oct. 2003, pp. 157–164.

[13] E. H. Land and J. J. McCann, "Lightness and retinex theory," *J. Opt. Soc. Amer.*, vol. 61, no. 1, pp. 1–11, 1971.

[14] J. Frankle and J. J. McCann, "Method and apparatus for lightness imaging," U.S. Patent 4 384 336, May 17, 1983.

[15] P. Soille, "Morphological operators," in *Handbook of Computer Visualization and Applications*, B. Jahne, H. Hauecker, and P. Geiler, Eds. San Diego: Academic, 1999, vol. 2, pp. 627–682.

[16] M. Elad, "Retinex by two bilateral filters" in *Scale Space and PDE Methods in Computer Vision* (Lecture Notes in Computer Science). R. Kimmel, N. Sochen, and J. Weickert, Eds., Berlin: Springer, 2005, vol. 3459, pp. 217–229.

[17] A. Wong, D. A. Clausi, and P. Fieguth, "Adaptive monte carlo retinex method for illumination and reflectance separation and color image enhancement," in *Proc. Can. Conf. Comput. Robot Vis.*, May 2009, pp. 108–115.

[18] T. Chen, W. Yin, X. Zhou, D. Comaniciu, and T. S. Huang, "Total variation models for variable lighting face recognition," *IEEE Trans. Pattern Anal. Mach. Intell.*, vol. 28, no. 9, pp. 1519–1524, Sep. 2006.

[19] G. Schaefer, M. I. Rajab, M. E. Celebi, and H. Iyatomi, "Colour and contrast enhancement for improved skin lesion segmentation," *Comput. Med. Imag. Graph.*, vol. 35, pp. 99–104, 2011.

[20] H. Iyatomi, M. E. Celebi, G. Schaefer, and M. Tanaka, "Automated color calibration method for dermoscopy images," *Comput. Med. Imag. Graph.*, vol. 35, pp. 89–98, 2011.

[21] P. G. Cavalcanti, J. Scharcanski, and C. B. O. Lopes, "Shading attenuation in human skin color images," in *Proc. 6th Int. Symp. Vis. Comput.*, 2010, pp. 190–198.
[22] J. Glaister, A. Wong, and D. A. Clausi, "Illumination correction in dermatological photographs using multistage illumination modeling for skin lesion analysis," in *Proc. EEE 34th Annu. Int. Conf. IEng. Med. Biol. Soc.*, Aug./Sep. 2012, pp. 102–105.
[23] A. Smith, "Color gamut transform pairs," *ACM SIGGRAPH Comput. Graph.*, vol. 12, no. 3, pp. 12–19, 1978.
[24] P. Fieguth, *Statistical Image Processing and Multidimensional Modeling*. New York, NY, USA : Springer-Verlag, 2011, p. 65.
[25] M. Chen, "Importance-weighted marginal Bayesian posterior density estimation," *J. Amer. Stat. Assoc.*, vol. 89, no. 427, pp. 818–824, Sep. 1994.
[26] P. W. Holland and R. E. Welsch, "Robust regression using iteratively reweighted least-squares," *Commun. Stat. Theor. Methods*, vol. A6, pp. 813–827, 1977.
[27] R. Nock and F. Nielsen, "Statistical region merging," *IEEE Trans. Pattern Anal. Mach. Intell.*, vol. 26, no. 11, pp. 1452–1458, Nov. 2004.
[28] B. Funt, F. Ciurea, and J. J. McCann, "Retinex in MATLAB," *J. Electron. Imag.*, vol. 13, no. 1, pp. 48–57, 2004.
[29] DermIS. (Dec. 4, 2012). [Online]. Available: http://www.dermis.net
[30] DermQuest. (Dec. 4, 2012). [Online]. Available: http://www.dermquest.com
[31] T. Fawcett, "An introduction to ROC analysis," *Pattern Recognit. Lett.*, vol. 27, no. 8, pp. 861–874, 2006.
[32] R. J. Friedman, D. S. Rigel, and A. W. Kopf, "Early detection of malignant melanoma: The role of physician examination and self-examination of the skin," *Cancer J. Clin.*, vol. 35, no. 3, pp. 130–151, 1985.
[33] C. Chang and C. Lin, "LIBSVM: A library for support vector machines," *ACM Trans. Intell. Syst. Technol.*, vol. 2, no. 3, pp. 27:1–27:27, 2011.
[34] E. Ardizzone, R. Pirrone, and O. Gambino, "Illumination correction on MR images," *J. Clin. Monit. Comput.*, vol. 20, no. 6, pp. 391–398, Jul. 2006.

Jeffrey Glaister (S'12) received the B.A.Sc. degree in systems design engineering from the University of Waterloo, Waterloo, ON, Canada, in 2011, where he is currently working toward the M.A.Sc. degree in systems design engineering.

He is a member of the Vision and Image Processing Research group. His current research topic is segmentation of skin lesions from dermatological photographs. His research interests include biomedical image processing, remote sensing, and pattern recognition.

Robert Amelard (S'11) received the B.S.E. degree in software engineering from the University of Waterloo, Waterloo, ON, Canada, in 2011, where he is currently working toward the M.A.Sc. degree at the Vision and Image Processing Lab, Department of Systems Design Engineering.

Before embarking on the postgraduate activities in computer vision, he held various software engineering positions in the fields of geospatial analysis, healthcare, finance, and advertising, as well as research positions in symbolic computation. His current research interests include medical image processing, remote sensing, and photogrammetry.

Mr. Amelard received the Sir Sandford Fleming Teaching Assistantship Excellence Award at the University of Waterloo.

Alexander Wong (M'05) received the B.A.Sc. degree in computer engineering, the M.A.Sc. degree in electrical and computer engineering, and the Ph.D. degree in systems design engineering from the University of Waterloo, ON, Canada, in 2010.

He is currently an Assistant Professor in the Department of Systems Design Engineering at the University of Waterloo. He has published refereed journal and conference papers, as well as patents, in various fields such as computer vision, graphics, image processing, multimedia systems, and wireless communications. His research interests include image processing, computer vision, pattern recognition, and cognitive radio networks, with a focus on biomedical and remote sensing image processing and analysis such as image registration, image denoising and reconstruction, image super-resolution, image segmentation, tracking, and image and video coding and transmission.

Dr. Wong has received the Outstanding Performance Award, the Engineering Research Excellence Award, the Early Researcher Award from the Ministry of Economic Development and Innovation, the Best Paper Award by the Canadian Image Processing and Pattern Recognition Society, and the Alumni Gold Medal.

David A. Clausi (S'93–M'96–SM'03) received the Ph.D. degree in systems design engineering from the University of Waterloo, Waterloo, ON, Canada, in 1996.

Afterward, he worked in software medical imaging at Agfa, Waterloo. He started his academic career in 1997 as an Assistant Professor in geomatics engineering at the University of Calgary, Calgary, Alberta, Canada. In 1999, he returned to his alma mater and is currently a Professor specializing in the fields of intelligent and environmental systems and was recently the Associate Chair—Graduate Studies. He is an active interdisciplinary and multidisciplinary researcher. He has an extensive publication record, publishing refereed journal and conference papers in the diverse fields of remote sensing, computer vision, algorithm design, and biomechanics. His research efforts have led to successful commercial implementations including creating, building, and selling his own company. He was the cochair of IAPR Technical Committee 7 Remote Sensing during 2004–2006.

Dr. Clausi has received numerous scholarships, paper awards, and two Teaching Excellence Awards. In 2010, he received the award for Research Excellence and Service to the Research Community by the Canadian Image Processing and Pattern Recognition Society.